



Effect of Rim and Web Thickness on Tooth Root Stress of Spur Gear

Jung-Ho Park¹ · Woo-Jin Chung¹ · Young-Jun Park^{1,2,3} · Heung-Sub Kim⁴ · Jin Beom Seo⁵ · Jong Sang Park⁵

Received: 26 May 2023 / Revised: 2 September 2023 / Accepted: 10 October 2023 / Published online: 10 February 2024
© The Author(s) 2024

Abstract

This study investigated the impact of spur gear rim and web thickness on root stress. A finite-element analysis model (FEM) was utilized and validated through a gear-bending test. Four gears with different rim and web specifications, including a solid gear, were designed and tested using strain gages to measure their root stress. The 3D FEM was validated by comparing the measured root stresses with that analyzed by the developed FEM. Using this model, a parametric study was conducted by varying the web position, pressure angle, and module to investigate the effect of the backup ratio on the root stress ratio of the gear. A stress-ratio map was generated based on the results. This stress-ratio map was compared with the rim thickness factor (Y_B) for external spur gears specified in ISO 6336-3. The comparison reveals that the rim thickness factor specified in ISO 6336 is overly conservative compared to values obtained in this study. Our results suggest that the thickness of both the rim and web should be considered to reduce the weight of spur gears. These findings can be applied to the design of lightweight spur gears.

Keywords External spur gear · Thinned-rim gear · Rim thickness · Web thickness · Light-weight design · FEA · Tooth root stress

List of Symbols

Y_B	Rim thickness factor in ISO standard
K_B	Rim thickness factor in AGMA standard
σ	Stress, MPa
E	Young's modulus, GPa
ϵ	Strain, m/m

1 Introduction

With the growing global concern regarding environmental degradation and conservation, strategies for enhancing energy and fuel efficiency through the reduction of materials in mechanical systems have drawn increasing interest; these strategies primarily focus on weight reduction. Numerous studies have aimed to address this challenge (Bian et al., 2015; Kroll et al., 2011; Solomon et al., 2020).

Furthermore, the improvement in gear efficiency in power transmission systems is an area of interest in the automotive and aviation sectors, where weight reduction is crucial for improving the fuel economy (Anderson & Loewenthal, 1982; Petry-Johnson et al., 2008; Simon, 1981; Xu et al., 2007). By reducing the weight of the gear—a critical component responsible for transmitting power—the fuel efficiency of the gearbox transmission can be enhanced, thereby yielding a greater weight reduction and energy efficiency (Joshi et al., 2014).

One of the most commonly applied methods for reducing gear weight involves optimizing the stress experienced by the gear teeth and the stiffness of the gear blanks through the reduction of the gear rim and web thickness (Opalic et al., 2011).

✉ Young-Jun Park
yjpark95@snu.ac.kr

¹ Department of Biosystems Engineering, Seoul National University, 1 Gwanak-ro, Gwanak-gu, Seoul 08826, Republic of Korea

² Research Institute of Agriculture and Life Sciences, Seoul National University, 1 Gwanak-ro, Gwanak-gu, Seoul 08826, Republic of Korea

³ Global Smart Farm Convergence, Seoul National University, 1 Gwanak-ro, Gwanak-gu, Seoul 08826, Republic of Korea

⁴ Department of Smart Industrial Machinery, Korea Institute of Machinery and Materials, 156 Gajeongbuk-ro, Yuseong-gu, Daejeon 34103, Republic of Korea

⁵ Hyundai Motor Company R&D Center, Hyundai Motor Company, Hwaseong-si, Gyeonggi-do 18280, Republic of Korea

However, reducing the rim and web thicknesses can increase the likelihood of gear breakage owing to the application of a greater stress to the root of the gear than the existing stress. Therefore, the changes in stress at the root of the gear must be considered when reducing the rim and web thicknesses.

To account for the increase in the root stress resulting from a decrease in the rim thickness, the international standard ISO 6336 (ISO, 2019) employs the rim thickness factor Y_B , from AGMA 2101 (American Gear Manufacturers Association, 1995) rim thickness factor K_B , without modification. However, these standards yield highly conservative values that do not significantly contribute to gear weight reduction.

Moreover, for gears with below a backup ratio of 0.5 (obtained by dividing the gear rim thickness by the height of the gear teeth), the rim thickness factor as suggested by these standards is not feasible. Additionally, no international standards are currently available that account for the increase in tooth root stress resulting from web thickness reduction.

Several studies have focused on experimental methods (gear-tooth bending test) and analytical methods (finite element analysis; FEA) to validate the changes in gear tooth root stress according to the rim thickness. Oda et al. (Oda et al., 1981) measured the stress of the tooth root by attaching strain gauges to the tooth root of spur gears with various rim thicknesses and verified the 2D finite-element analysis model (FEM) modeled as a triangular element using the test results. To confirm the validity of the single-tooth model, the stress analysis results of the tooth root of the single-gear and adjacent-gear tooth models were compared. However, the 2D FEM model involved a limitation: the gear tooth root stress resulting from the web change was not considered.

Arai et al. (1981) conducted the static bending and bending fatigue tests to confirm the fatigue limits of solid and thin rim gears with holes. These tests revealed that the bending fatigue limit significantly decreased for values where the ratio of rim thickness to modulus was 2.5.

In contrast, Bibel et al. (1994) performed an FE analysis using a five-tooth gear model. The gear rim thickness was divided into eight equal parts to create the FE model, and a thin-rim thickness model was created by gradually removing the rim thickness from the analytical model.

With the model generated using this method, they validated the inflection point by generating a graph of the maximum tension and compression according to the ratio of tooth height to rim thickness. The maximum compressive and alternating stresses increase when the backup ratio is 1.3 or less.

Drago and Pizzigati (1980), Drago and Lutthans () measured the tooth root stress using three test gears with different rim thicknesses using the photoelastic method. Because the data were obtained with a limited number of test gears, the

rim thickness factor, K_B , for backup ratios from 0.5 to 2.0 was presented by extrapolating the measured test data.

However, the study conducted by Drago et al. was limited to plastic gears and did not involve metal gears. Furthermore, the research focused only on the rim thickness without considering the thickness of the gear web.

The maximum point of tooth root stress generation calculated using the aforementioned international standards varies depending on the application theory of each standard and differs from the actual maximum point of tooth root stress generation that occurs in real gears.

In addition, the cited studies (Arai et al., 1981; Bibel et al., 1994; Drago & Pizzigati, 1980; Drago & Lutthans, 1983a, 1983b; Oda et al., 1981) did not verify the FE analysis results through tests; this resulted in a limitation—these studies could not be analyzed with a model showing the same root stress characteristics as the actual gear.

To address these research limitations, the current study accurately predicted the point where the maximum tooth root stress occurs in gears; a high-fidelity 3D FEM was developed and validated through root stress testing of gear teeth to analyze the tooth root stress of gears with thin rims and webs.

In this study, the effects of changes in the rim and web thicknesses on the root stress of gear teeth in spur gears were analyzed experimentally and analytically.

Based on a root-stress analysis model for gear teeth validated through experiments, this study presents a stress ratio, defined as the ratio of the maximum stress of gears with thickness changes in the rim and web to the maximum stress of solid gears according to the backup ratio. Four types of gears were manufactured: solid gears, gears with thin rims, gears with thin webs, and gears with intermediate rims and webs.

A load was applied to the highest point of the single-tooth contact (HPSTC) of each gear, and strain gauges were attached to the gear tooth root to measure the actual gear tooth root stress.

In contrast to previous studies, 3D FEMs were developed for each gear, and their high fidelity was confirmed through comparison with the experimental results.

Based on the developed model, a parametric study was conducted to analyze the stress ratio based on the backup ratio, considering the effects of changes in the web position, pressure angle, and module.

Moreover, the stress ratios obtained from the developed model were analyzed for different backup ratios by conducting a parametric study on the web position changes, pressure angle variations, and module changes. In addition, the stress-ratio map obtained in this study was compared with the rim thickness factor presented in the ISO 6336 standard to obtain stress ratios for gears with backup ratios of 0.3, which are not covered in the ISO 6336 standard.

2 Experimental Study

2.1 Manufacturing Test Gears and Bending Test Rig

To experimentally analyze the effect of rim and web thicknesses on gear tooth root stress, designing and manufacturing test gears with different rim and web thicknesses, as illustrated in Fig. 1 and described in Table 1, the blank shapes of the test gears are presented in Fig. 2. Four types of test gears were designed and manufactured for this study: (a) a solid gear with no rim or web, (b) a reference gear with a web thickness ratio of 0.5 and a backup ratio of 1, (c) a gear with the same web thickness ratio as the reference gear but with a backup ratio of 0.5, and (d) a gear with a web thickness ratio of 0.25 and the same rim thickness as the reference gear. The web thickness and backup ratios are defined in Eqs. (1) and (2), respectively.

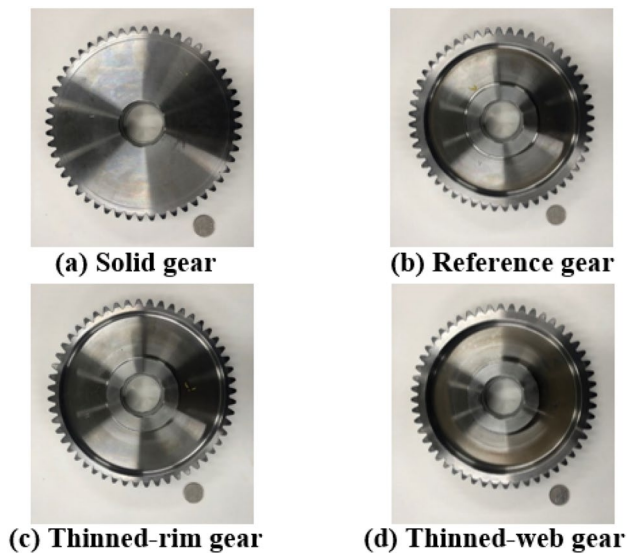


Fig. 1 Test gears used in this study

Table 1 Geometry and specification of test gears

Parameters	Units	Solid gear	Reference gear	Thinned-rim gear	Thinned-web gear
Number of teeth	[-]	52	52	52	52
Normal module	[mm]	4	4	4	4
Pressure angle	[deg]	20	20	20	20
Web thickness ratio	[-]	-	0.5	0.5	0.25
Back-up ratio	[-]	-	1	0.5	1
Young's modulus	[GPa]	210	210	210	210
Poisson's ratio	[-]	0.3	0.3	0.3	0.3
Face width	[mm]	40	40	40	40
Tooth height	[mm]	9.4	9.4	9.4	9.4
Quality (ISO 1328:2013)	[-]	6	6	6	6

Based on the method presented in ISO 6336-3 Tooth Root Stress Method B (ISO 6336-3, 2019), a gear tooth bending test device was fabricated and utilized for conducting gear-root stress measurements. To apply a line load to the HPSTC, the location where the gear root stress is maximized, a symmetric test jig was fabricated and employed, as presented in Figs. 3 and 4. In gear-bending tests, the number of gear teeth that can be subjected to a load varies depending on the size, characteristics, and gear specifications. Based on the 2D computer-aided design (CAD) model shown in Fig. 3, which was used to validate the specifications of the test gear used in this study, it was determined that in order to apply a line load to the desired location of the HPSTC, seven gear teeth must be symmetrically fixed. Therefore, a test apparatus was designed, as visualized in Fig. 4, to accommodate the seven gear teeth, and a gear tooth bending test was conducted, as depicted in Fig. 5. The gear-bending test rig was designed and manufactured in accordance with specifications reported in the literature (Meneghetti et al., 2018).

$$\text{Web thickness ratio} = \frac{\text{Gear web thickness}}{\text{Gear face width}} \tag{1}$$

$$\text{Backup ratio} = \frac{\text{Gear rim thickness}}{\text{Gear tooth height}} \tag{2}$$

2.2 Strain Gauge Attachment on Test Gears

An FEA was performed when a load was applied to the HPSTC, as illustrated in Fig. 6a, to validate the location where the maximum stress occurred at the root of the gear tooth. All four test gears illustrated in Fig. 1 exhibited similar maximum tooth root stress locations.

Based on the analysis results, six strain gauges were attached along the gear lead direction at the gear root

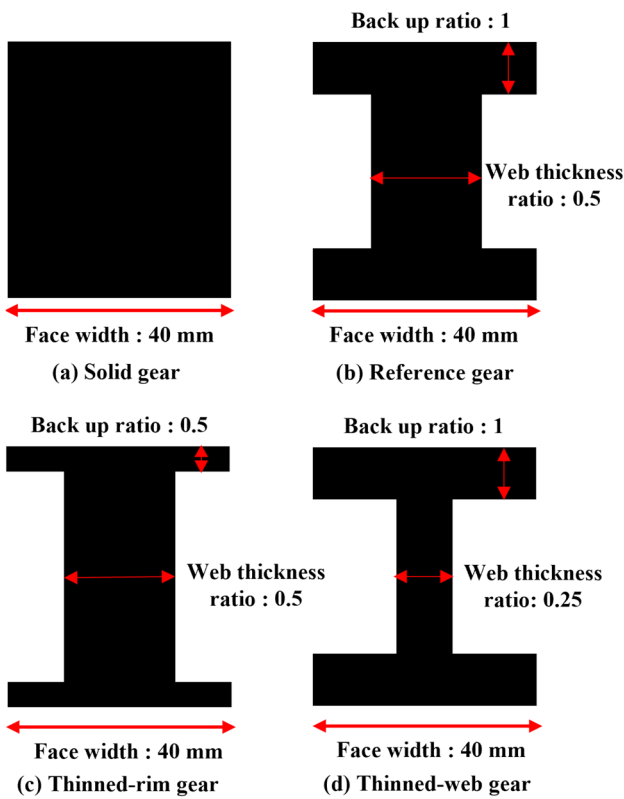


Fig. 2 Blank shapes of test gears

location where the maximum tooth root stress occurred, as depicted in Fig. 6b. As shown in Fig. 6c, strain gauges

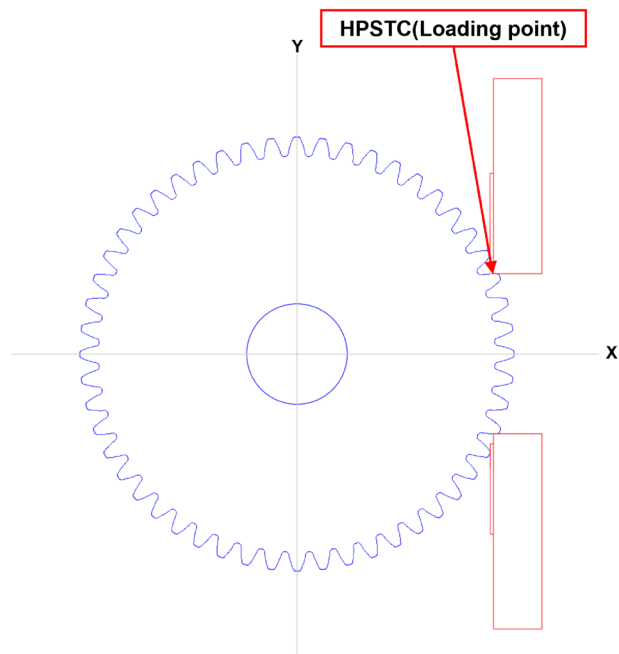


Fig. 3 Loading point for gear tooth bending test

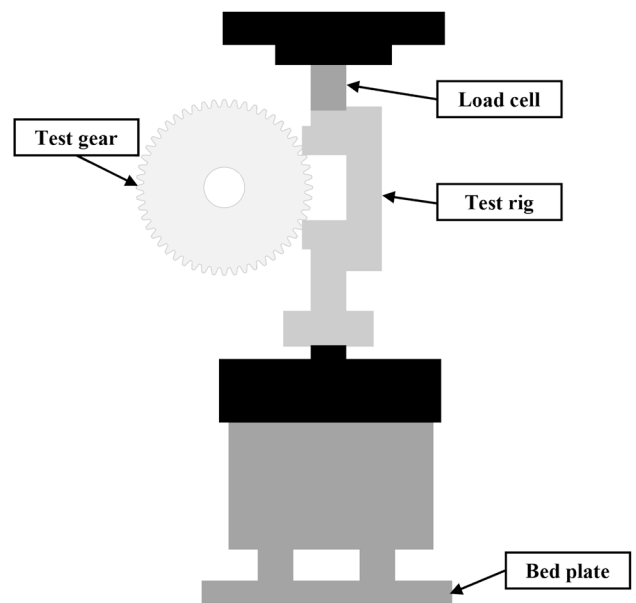


Fig. 4 Schematics of gear tooth bending test device for measuring gear root stress

were attached to two root positions with a phase difference of 180° per test gear, as visualized in Fig. 6d, and the root stress of the gear tooth was measured accordingly.

The specifications of the strain gauges used in these tests are listed in Table 2. SAE J 1619 (SAE International, 2017) and SAE J 821042 (SAE International, n.d.) were employed as the strain gauge attachment methods.

2.3 Measuring and Analyzing Gear Tooth Root Stress

MTS 810 model was used for the gear tooth bending test device, and its specifications are listed in Table 3. The data acquisition system comprised a UCAM 550-A (KYOWA)

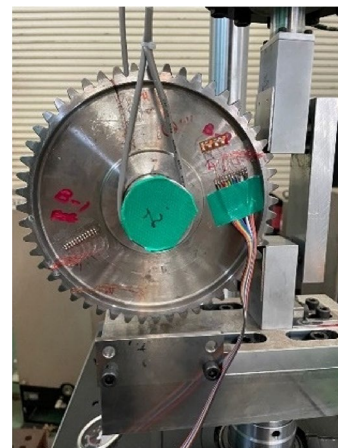


Fig. 5 Gear tooth bending test device for measuring gear root stress

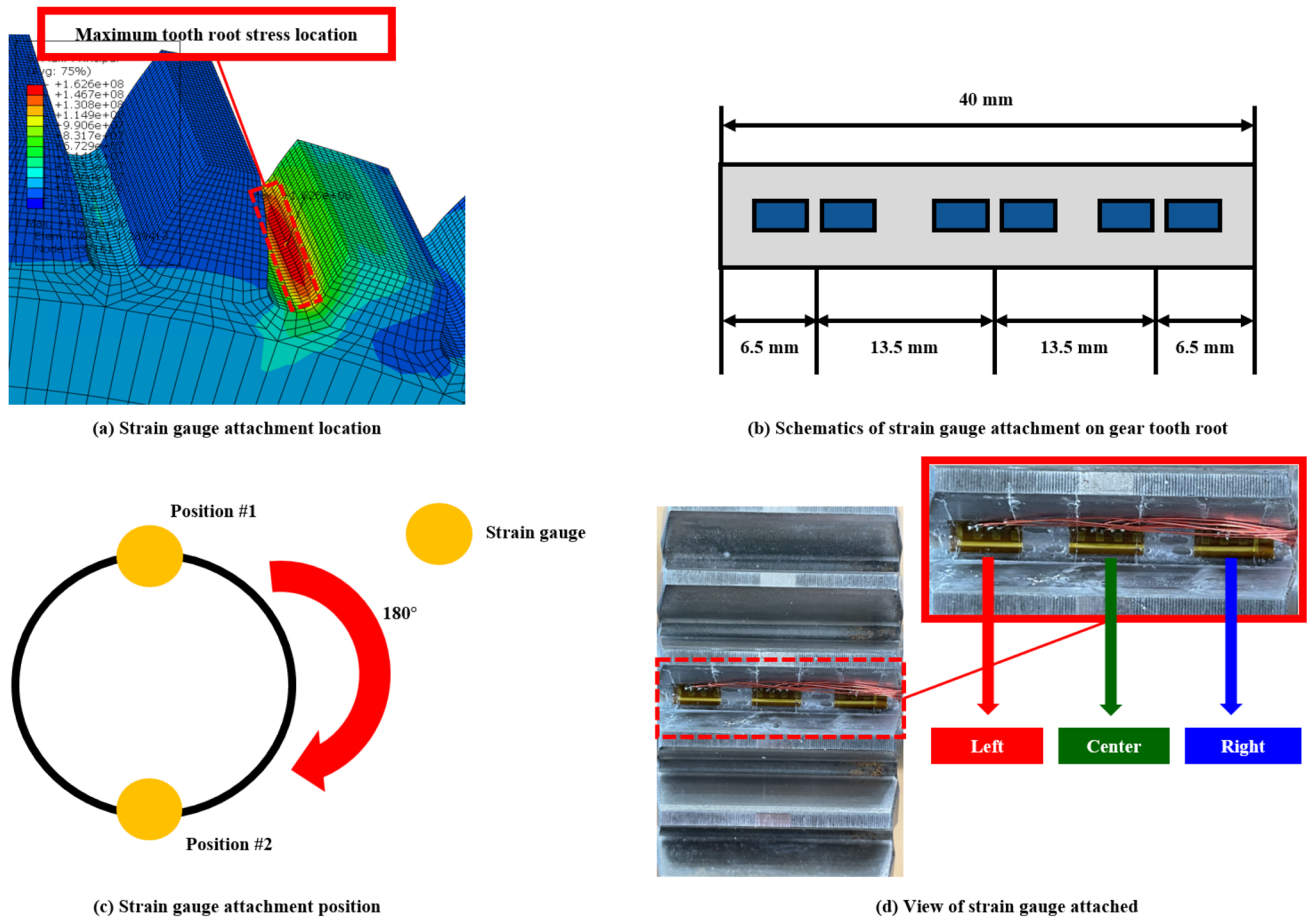


Fig. 6 Mounting position of strain gauges on gear tooth root

Table 2 Specification of strain gauge used in this study

Parameters	Units	Strain gauge
Model	[-]	EA-06-031MF-120
Resistance	[Ω]	120
Gauge length	[mm]	0.79
Overall length	[mm]	23.9
Overall width	[mm]	4.8

Table 3 Specification of test device on gear tooth bending

Parameters	Units	Gear tooth bending test device
Model	[-]	MTS 810
Force range	[kN]	- 50 to 50
Vertical test space	[mm]	1308
Working height	[mm]	889
Stiffness	[N/m]	2.6×10^8

for collecting the measurement data representing the stress levels at the roots of the gear teeth, and the device specifications are listed in Table 4. Six strain gauges were attached to the gear root, as illustrated in Fig. 6b, and strains were measured in sets of two in the lead direction at the left, center, and right positions of the gear tooth width, as depicted in Fig. 6d (SAE International, 2017). In the gear tooth bending test, the load was linearly increased from 0 to 10 kN, and the gear tooth root strain was measured accordingly. Equation (3) was used to convert the strain into stress values.

$$\sigma = E\epsilon. \tag{3}$$

Table 4 Specification of data acquisition system on gear tooth bending test

Parameters	Units	Data acquisition system
Model	[-]	KYOWA UCAM-550A
Channels	[channels/unit]	Maximum of 50
Sampling Frequencies	[Hz]	1, 2, 10, 20, 50
Accuracy	[%]	±0.05
Operating temperature range	[°C]	0 to 40

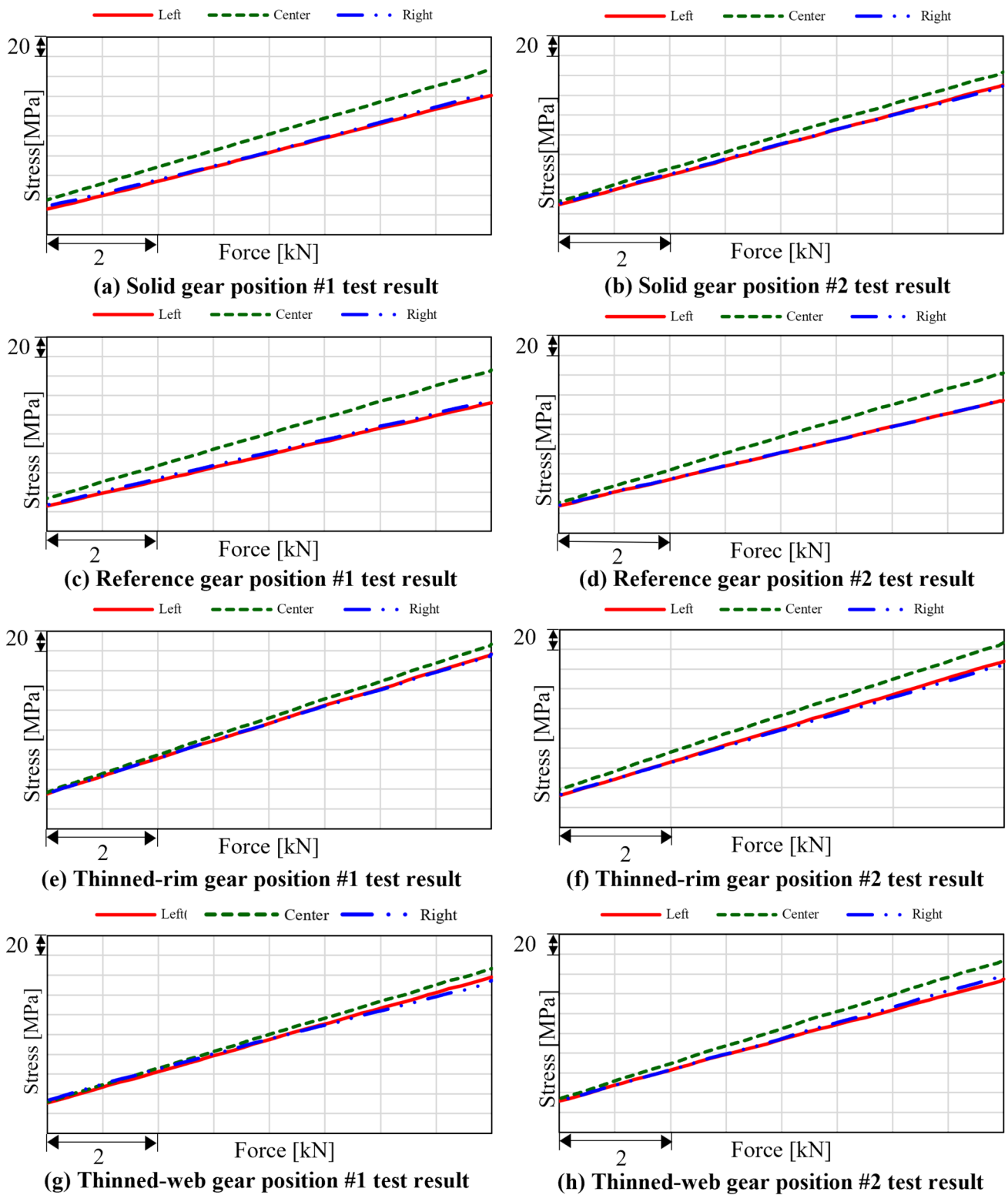


Fig. 7 Stress results of gear tooth bending test

Here, σ represents the gear root stress (MPa), E represents the Young's modulus of the gear material (GPa), and ϵ represents the measured strain (m/m).

The bending test results of the test gears, as plotted in Fig. 7, reveal that the maximum stress occurred at the center of the tooth width for all the test gears.

Table 5 Comparison of the ratio between the center results of solid gear position #1 and the test results

Parameters	Solid gear		Reference gear		Thinned-rim gear		Thinned-web gear	
	Position #1	Position #2	Position #1	Position #2	Position #1	Position #2	Position #1	Position #2
Left ratio	0.93	0.85	0.82	0.87	1.09	1.04	0.98	0.98
Center ratio	1.00	0.99	1.03	1.00	1.15	1.16	1.02	1.08
Right ratio	0.91	0.86	0.84	0.83	1.08	1.02	0.93	0.96

Table 6 Material properties of gear the FEM

Parameters	Units	Gear
Material	[-]	Alloy Steel
Young’s modulus	[GPa]	210
Poisson’s ratio	[-]	0.3
Yield strength	[MPa]	365
Tensile strength	[MPa]	517

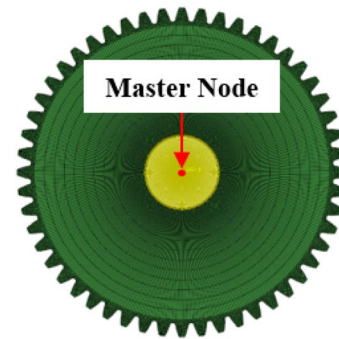
Table 7 Specifications of the gear FEMs

Parameters	Number of elements	Number of nodes
Solid gear	765,440	850,669
Reference gear	840,320	937,197
Thinned-rim gear	765,440	860,653
Thinned-web gear	811,200	912,237

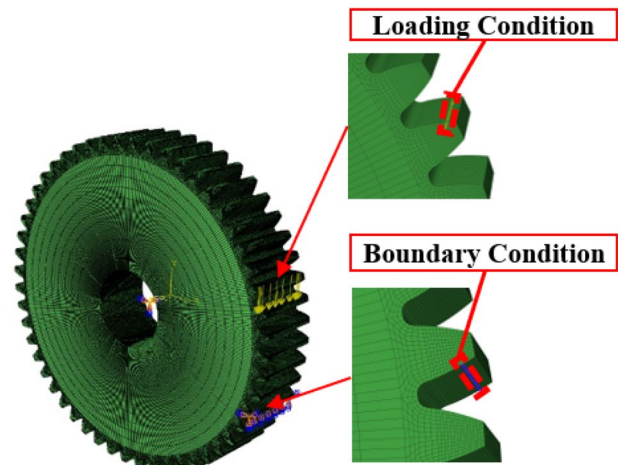
Upon analyzing the tooth root bending test results of the four test gears, it was found that the stress deviation at the left and right positions of the tooth width was not considerably large. These results indicate that edge contact or contact misalignment did not occur during the gear tooth bending test.

The difference in stress at the gear root at positions 1 and 2 with a 180° phase difference, as depicted in Fig. 6c, is insignificant. The test results in Fig. 7 are reported in Table 5 as the ratio of the center stress at position 1 of the solid gear. The reference gear with a backup ratio of 1 and web thickness ratio of 0.5 showed insignificant differences at the left, right, and center positions when compared to the stress of the solid gear.

Upon comparing the stress between the thinned-web gear with a backup ratio of 1 and web thickness ratio of 0.25 and the solid gear, an insignificant difference in stress was observed at the center position. However, the stress at the left and right positions of the thinned-web gear increased significantly compared with that of the solid gear.



(a) FE gear constrained condition



(b) FE gear loading condition

Fig. 8 Loading and boundary conditions for gear FEA

For the thinned-rim gear with a backup ratio of 0.5 and a web thickness ratio of 0.5, the stresses at the left, right, and center positions increased considerably compared to those for the solid gear.

The test results revealed that the stress of the gear increased significantly only at the left and right positions when the web thickness ratio was 0.25, whereas when the backup ratio was 0.5, the stress at the left, right, and center positions increased significantly.

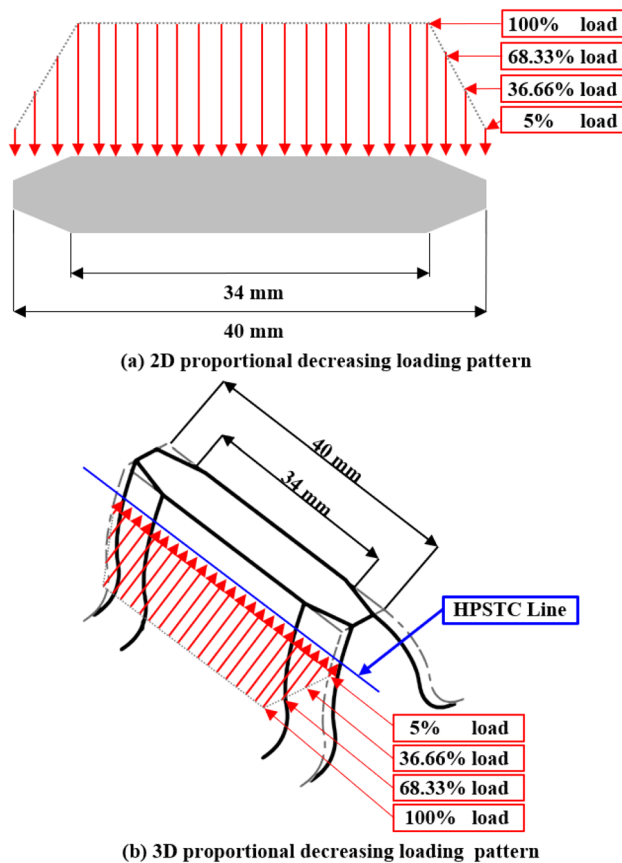


Fig. 9 Proportionally decreasing loading-condition pattern considering end relief

3 Results and Validation of the FE Model for Gear Tooth Root Stress

3.1 FE Modeling for Analyzing Gear Tooth Root Stress

A gear FEM was developed using Abaqus/CAE (Dassault Systems, 2013) to predict the gear-tooth root stress with respect to changes in the gear rim and web geometry. The FE element used in the gear FEM, a linear brick element (C3D8) with eight nodes and six faces, was utilized in accordance with previous studies (Chen & Tsay, 2002; Li, 2002). The material properties of the gear FEM are listed in Table 6.

To apply a load to the gear HPSTC and determine the point of maximum gear-tooth root stress, the gear FEM generated a fine gear-tooth mesh. To investigate the stress difference owing to changes in the web thickness and web position, a fine mesh was generated for the face width of the gear. The details of the developed gear FEM are listed in Table 7.

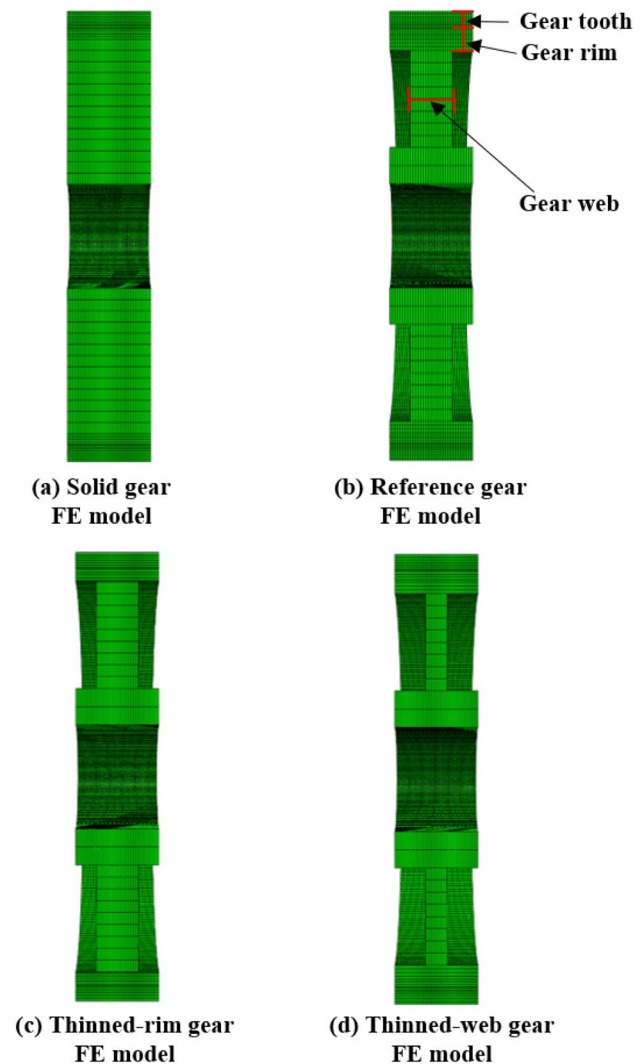


Fig. 10 Blank shapes for developed FE model

Moreover, to characterize the gear-tooth root stress, loading and boundary conditions were applied, as illustrated in Fig. 8a. The nodes on the inner surface of the gear are coupled to the master nodes, which are subsequently restrained to five degrees of freedom, except in the rotational direction. The gear loading condition, as depicted in Fig. 8b, is established as follows: to implement the same analysis conditions as the test conditions, a load was applied to the HPSTC point of the gear, and the nodes at the X-axis symmetric point in Fig. 3 were restrained in all degrees of freedom.

The tested gear has end reliefs measuring 3 mm on each side of the gear face, as shown in Fig. 9. To reflect the effect of the end relief applied to the gear, a linearly decreasing load was applied toward the left and right ends at the point

Table 8 Comparison between FEA results and test results

Parameters	Units	Solid gear		Reference gear		Thinned-rim gear		Thinned-web gear	
		Position #1	Position #2	Position #1	Position #2	Position #1	Position #2	Position #1	Position #2
Left error	[%]	1.93	-6.98	-10.87	-4.8	16.64	12.74	9.1	9.3
Center error	[%]	-0.98	-1.88	-1.2	-4.56	1.61	2.81	-2.47	3.32
Right error	[%]	-0.03	-6.42	-8.53	-9.05	16.17	10.96	4.52	7.11

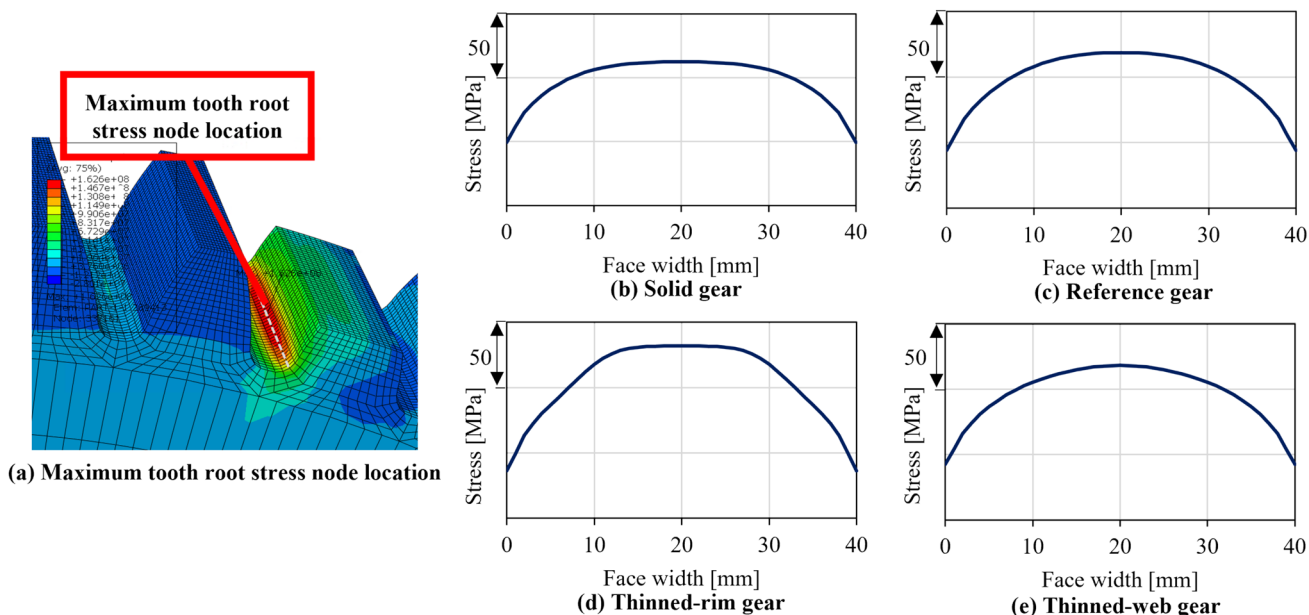


Fig. 11 FEA results of maximum tooth-root stress according to gear face width

Fig. 12 Maximum stress point of target gears

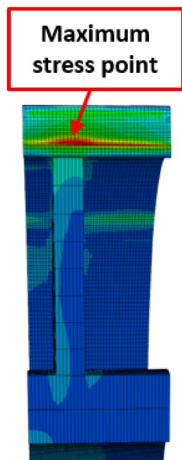


Table 9 Parametric study cases

Parameters	Model	Web position	Pressure angle	Module
Reference	A	0	20	4
Web position variation	B	0.5	20	4
	C	1	20	4
	D	0	16	4
Pressure angle variation	E	0	18	4
	F	0	20	2
Module variation	G	0	20	3

3.2 Validation for Gear FE Model

Table 8 lists the relative errors between the measured stresses at positions 1 and 2, as illustrated in Fig. 6c, and stress obtained via FEA. The relative error was calculated using Eq. (4).

$$\text{Relative error} = \frac{\text{Test Result} - \text{FEA result}}{\text{Test result}} \tag{4}$$

where the end relief began. This proportional load reduction was determined through trial and error by comparing the analysis and test results of the solid gear. Blank shapes of the four tested gears were generated using the FEM, as depicted in Fig. 10.

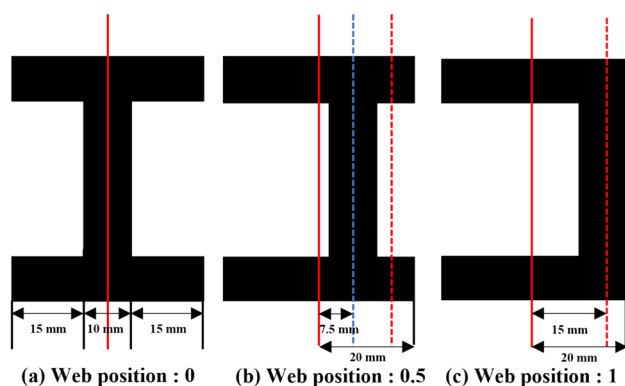


Fig. 13 Definition of gear web position

The maximum values of the relative errors of the center and end points of the face width (face width: 0–10 mm and 30–40 mm) analyzed for the four test gears were 4.56% and 16.64%, respectively, which were well correlated.

The maximum error occurred in the thinned-rim gear, which was 50% thinner than the reference gear. As shown in Fig. 11b–e, the stress variation with respect to the face width position exhibited a higher magnitude at the end point (0–10 mm; 30–40 mm) of the face width than at the center point (10–30 mm) of the face width. In particular, the stress variation in the thinned-rim gear (Fig. 11d) was significantly larger than that in magnitude compared to the other tested gears.

This result implies that a small error in the attachment position of the strain gauges during the gear root stress measurement can lead to a significant increase in the relative error between the measured and analyzed stresses. These results conclusively indicate that large relative errors occurred at the left and right positions of the thinned-rim gear.

4 Parametric Study & Results Using Gear FE Model

Based on the verified FE model, the stress ratios of the gear roots were analyzed with respect to the backup ratio by varying the web position, pressure angle, and the number of modules. The stress ratio of the gear roots is defined using Eq. (5).

$$\text{Stress ratio} = \frac{\text{maximum gear tooth root stress of target gear}}{\text{maximum gear tooth root stress of solid gear}} \quad (5)$$

The stress ratio is calculated using the maximum root stress, which is the most critical factor affecting the gear failure. As demonstrated in Fig. 12, the maximum tooth root stress point and stress values are obtained through FEA.

A parametric study was conducted for variations in the web position, pressure angle, and module, and the results are presented in the form of a stress-ratio map in Table 9.

In each model, the web thickness ratios (Eq. 1) was varied at four types (0.2, 0.4, 0.6, and 0.8), and the backup ratio (Eq. 2) was varied at eleven types (0.3, 0.4, 0.5, 0.6, 0.7, 0.8, 0.9, 1, 1.2, 1.5, and 2.0). Therefore, 308 FEA simulations were conducted in this parametric study.

The x-axis of the graphs (parametric study results) presented in Figs. 14, 15 and Fig. 16 represents the backup ratio, whereas the y-axis represents the stress ratio for each parametric study case. In each figure, the numbers following the model name (e.g., A-1, A-2, A-3, and A-4) represent the web thickness. A smaller value indicates a smaller web thickness factor.

4.1 Parametric Study #1: Web Position Variation

In this study, the module was fixed at 4, and the pressure angle was fixed at 20°. As shown in Fig. 13, parametric studies were performed for three different web positions.

As shown in Fig. 14, the stress ratio increased as the backup ratio decreased when the backup ratio was less than 1.0, and the stress ratio increased rapidly when the backup ratio was less than 0.5.

Considering the web thickness and backup ratio simultaneously, the stress ratio increased by more than 20% when the backup ratio was 0.5 or less and the web thickness ratio was 0.4 or less.

As shown in Fig. 12, as the web position was changed to 0.5 and 1 to obtain an asymmetric gear blank, the maximum stress of the gear occurred at the point wherein the web and rim met and not at the midpoint of the tooth width. Additionally, the maximum stress increased by 1.3% compared to that for gears with symmetrical blanks featuring webs in the middle.

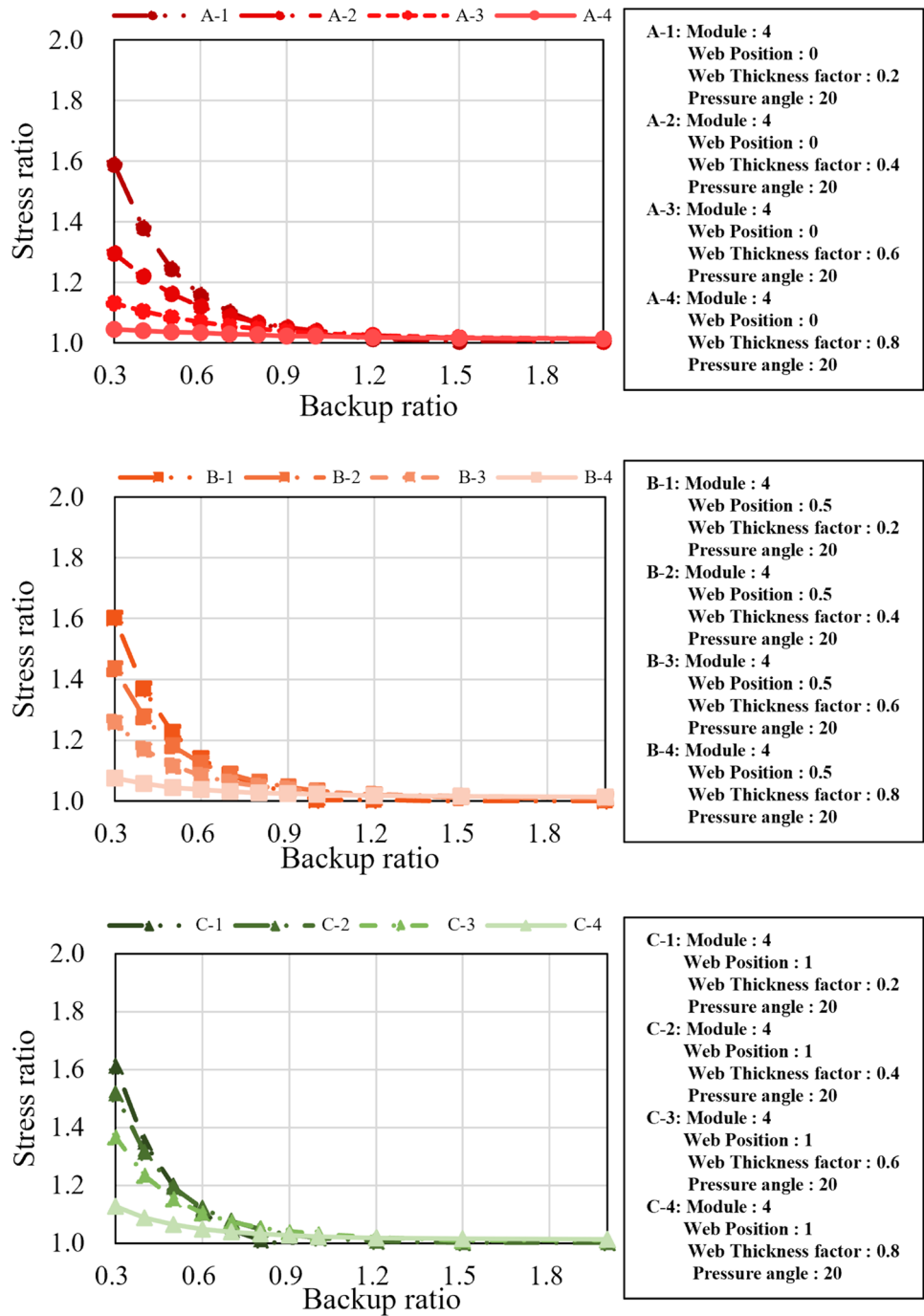
4.2 Parametric Study #2: Pressure Angle Variation

In this study, the module was fixed at 4 and the web position at 0. Parametric studies were performed at three different pressure angles (16°, 18°, and 20°).

As plotted in Fig. 15, the difference in the maximum tooth-root stress according to the pressure-angle change in the range of 16°–20° was approximately 1%, which was insignificant.

The variation in the pressure angle during changes in the rim and web thickness implies that it does not have a significant impact on the variation in the maximum root stress. Similar to the results of the parametric study based on the web-position change performed previously, the

Fig. 14 Stress-ratio map according to web position variation



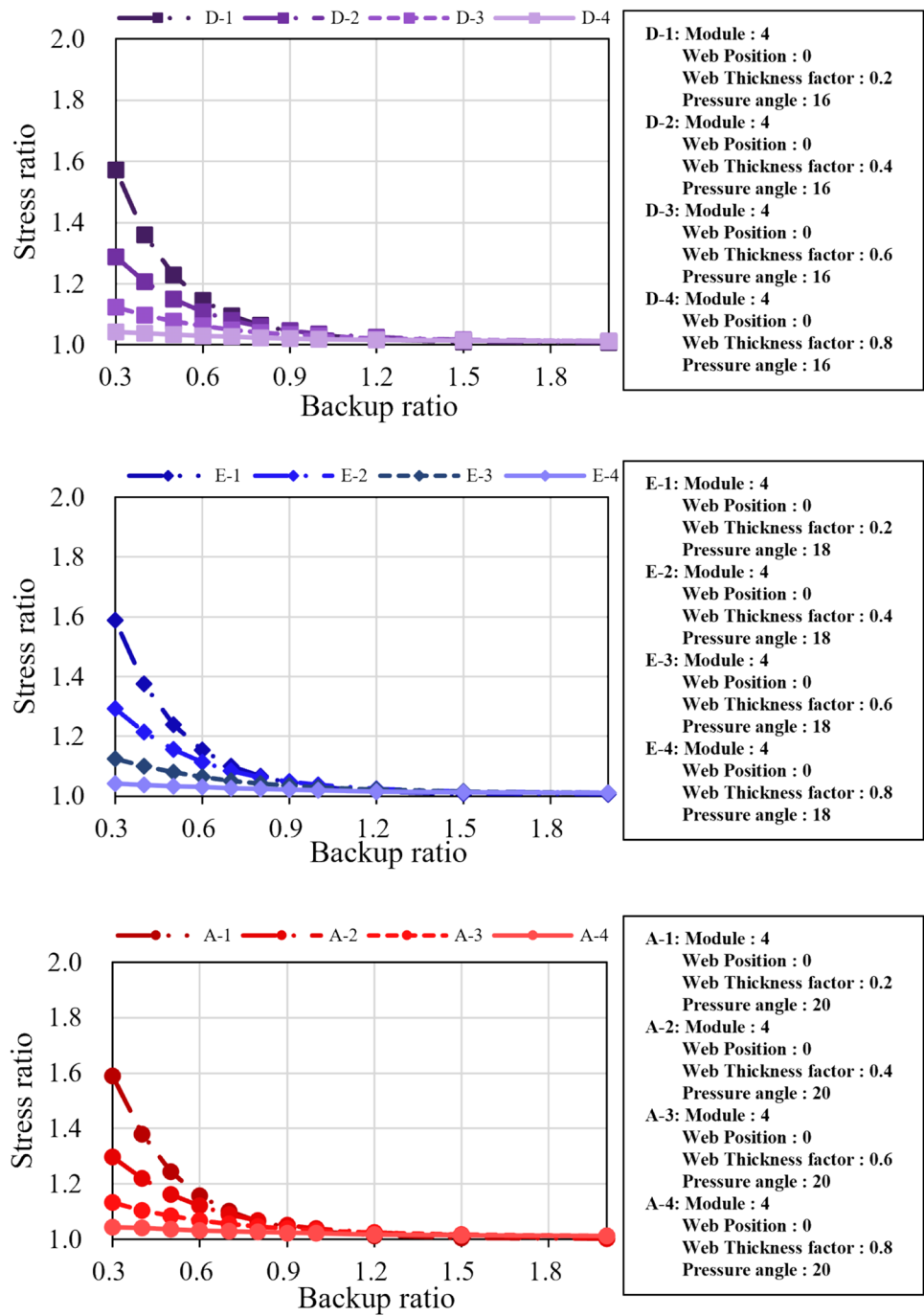
stress ratio increased rapidly when the backup ratio was less than 0.5.

Considering the backup ratio and web thickness simultaneously, the stress ratio increased rapidly when the backup ratio was less than 0.5 and the web thickness ratio was less than 0.4.

4.3 Parametric Study #3: Module Variation

The pressure angle was fixed at 20°, and the web position was set to 0. Parametric studies were performed using three different modules (2, 3, and 4).

Fig. 15 Stress-ratio map according to pressure angle variation

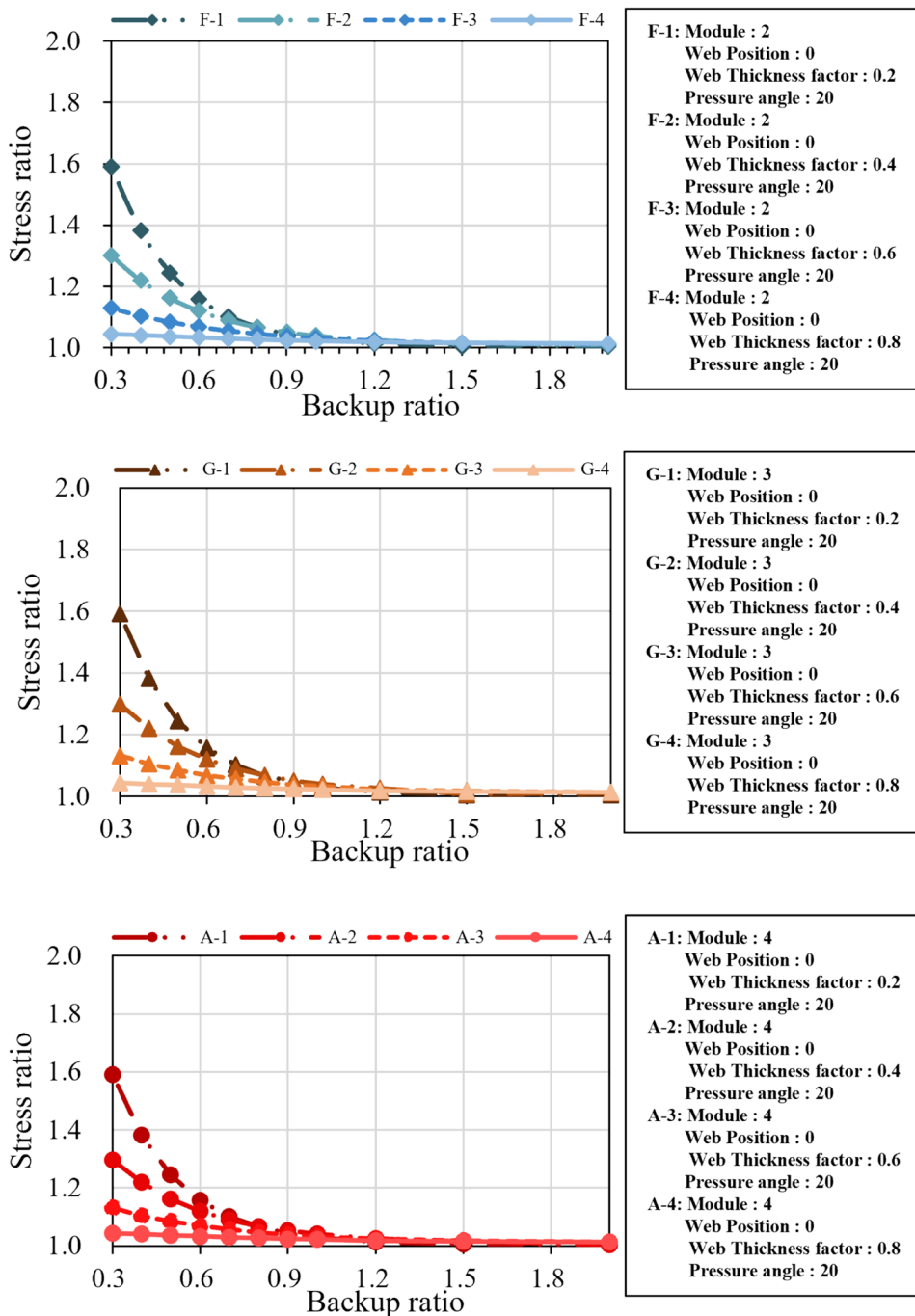


As indicated in Fig. 16, no variation occurred in the maximum root-stress ratio despite the change in the module; only a difference in the absolute stress values was manifested.

Similar to the results of the previous parametric study based on web-position variation and pressure-angle variation, the stress ratio increased rapidly when the backup ratio was less than 0.5.

Considering both the rim thickness and web thickness simultaneously, the stress ratio increased rapidly when the backup ratio was less than 0.5 and the web thickness ratio was less than 0.4.

Fig. 16 Stress-ratio map according to module variation



5 Comparison Between ISO 6336 Standard and Stress-Ratio Map

Figure 17 presents a comparison between the stress-ratio map of the web position variation, pressure angle variation, and module variation, and the Y_B factor graph, which indicates the rim thickness factor of the external gears presented in ISO 6336-3.

In the rim thickness factor presented in ISO 6336-3, the stress ratio started to increase from a back-up ratio of 1.2. Moreover, the stress-ratio map based on web position variation, pressure angle variation, and module variation performed in this study revealed that the back-up ratio increased from 1.0. Furthermore, the Y_B factor presented in ISO 6336-3 was extremely conservative when compared with the stress-ratio map of the parametric study conducted in this study.

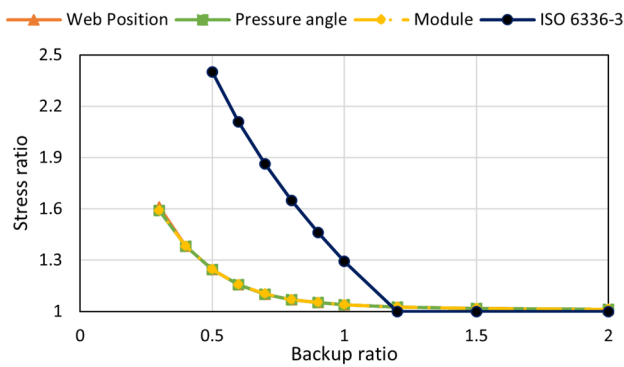


Fig. 17 Comparison between parametric stress-ratio map and ISO 6336 results

6 Conclusion

In this study, the effects of the rim and web thicknesses of a spur gear on the tooth-root stress were analyzed using a FEM that was verified through testing.

For the FEM validation test, a gear tooth bending test device was implemented based on ISO 6336-3 Tooth root stress Method B (ISO, 2019) and the test device of Meneghetti et al. (2018). Four test gears (solid, reference, thinned-rim, and thinned-web gears) were designed and manufactured to measure the tooth root stress for FEM validation.

After detecting the point of maximum tooth-root stress predicted through FEA, the stress at the tooth root was measured by attaching a strain gauge to the point.

Comparing the measured gear tooth-root stress data and the analyzed values of the developed FEM, revealing that the FEM reflected the test results well, with an error range of the gear center-tooth root stress of 0.98–4.56%.

Using the developed 3D FEM, a parametric study was performed on the change in the gear tooth-root stress for varying thicknesses of the spur gear rim and web according to the variations in the web position, pressure angle, and module.

The results obtained from the stress-ratio map of the parametric study for web position variation, pressure angle variation, and module variation are as follows:

- (1) When the web position of the gear was moved from the center to the left or right to create an asymmetric blank, the point where the maximum tooth root stress occurred changed from the center to the position where the web was moved. The maximum tooth-root stress of gears whose web position was moved to the left or right instead of the center increased by 1.3% compared with those of gears whose webs were moved to the center.

When designing gears with asymmetrical gear-blank shifting of the web position, the increase in the maximum stress point along with the change in the maximum tooth-root stress point must be considered.

- (2) The stress ratio tendency was analyzed according to the variation in pressure angle (16°, 18°, and 20°), revealing that the maximum stress difference between the backup ratio of 0.3 and web thickness ratio of 0.2, where the largest stress occurred in the parametric study case, was approximately 1%. Therefore, a pressure angle change from 16° to 20° had an insignificant effect on the change in the tooth root stress between the gears.
- (3) Upon analyzing the stress ratio against the backup ratio according to the module change (3, 4, 5), no change was observed in the stress ratio, except for the difference in the absolute value of stress, due to the application of the same load.
- (4) A common result obtained from the three parametric studies was that the stress ratio started increasing at a backup ratio of 1.0. From the point where the web thickness ratio was less than 0.4 and the backup ratio was less than 0.5, the stress ratio increased sharply.
- (5) Upon comparing the stress-ratio maps obtained for different web positions, pressure angles, and modules with the rim thickness factor (Y_B) presented in ISO 6336-3, the Y_B factor in ISO 6336-3 was found to be more conservative than the results obtained in this study. While ISO 6336-3 provides a Y_B factor that can predict stress ratios for gears with backup ratios greater than 0.5, this study reports stress ratios for gears with backup ratios as low as 0.3.
- (6) This study demonstrates that to reduce the weight of the spur gear, mutual consideration of the rim and web thicknesses is necessary when reducing the thickness of the rim and web. The results of this study can serve as fundamental data for establishing lightweight design standards for spur gears. However, the study was conducted under the assumption of a uniform load acting on the gear, and gear-mesh misalignment or gear-edge contact phenomena were not considered. Further studies are planned to analyze the effect of gear tooth-root stress on the rim and web thickness under the conditions of gear-mesh misalignment or gear-edge contact.

Acknowledgements This work was supported by Hyundai Motor Company.

Funding Open Access funding enabled and organized by Seoul National University.

Data Availability Data sets generated during the conduct of this study are available from the corresponding author upon reasonable request, in compliance with Hyundai Motor Company's Data Protection Regulation to ensure the protection and confidentiality of the data.

Open Access This article is licensed under a Creative Commons Attribution 4.0 International License, which permits use, sharing, adaptation, distribution and reproduction in any medium or format, as long as you give appropriate credit to the original author(s) and the source, provide a link to the Creative Commons licence, and indicate if changes were made. The images or other third party material in this article are included in the article's Creative Commons licence, unless indicated otherwise in a credit line to the material. If material is not included in the article's Creative Commons licence and your intended use is not permitted by statutory regulation or exceeds the permitted use, you will need to obtain permission directly from the copyright holder. To view a copy of this licence, visit <http://creativecommons.org/licenses/by/4.0/>.

References

- AGMA. (1995). *2101–C95, Fundamental Rating Factors and Calculation Methods for Involute Spur and Helical Gear Teeth*. Alexandria: American Gear Manufacturers Association.
- Anderson, N. E., & Loewenthal, S. H. (1982). Design of spur gears for improved efficiency. *ASME Journal of Mechanical Design*, *104*(10), 767–774.
- Arai, N., Harada, S., & Aida, T. (1981). Research on bending strength properties of spur gears with a thin rim. *Bulletin of JSME*, *24*(195), 1642–1650.
- Bian, J., Mohrbacher, H., Zhang, J. S., Zhao, Y. T., Lu, H. Z., & Dong, H. (2015). Application potential of high performance steels for weight reduction and efficiency increase in commercial vehicles. *Advances in Manufacturing*, *3*, 27–36.
- Bibel, G. D., Reddy, S. K., Savage, M., & Handschuh, R. F. (1994). Effects of rim thickness on spur gear bending stress. *Journal of Mechanical Design*, *116*(4), 1157–1162.
- Chen, Y. C., & Tsay, C. B. (2002). Stress analysis of a helical gear set with localized bearing contact. *Finite Elements in Analysis and Design*, *38*(8), 707–723.
- Drago, R. J., & Lutthans, R. V. (1983a). Combined effects of rim thickness and pitch diameter on spur gear tooth stresses. *Journal of the American Helicopter Society*, *28*(3), 13–19.
- ISO 6336-3. (2019). *Calculation and load capacity of spur and helical gears*. International Organization for Standardization.
- Joshi, S. S., Pushparaj, C. M. A., & Jaykarthikeyan, P. V. (2014). Transmission weight & efficiency optimization in off road vehicle (Tractor Gearbox). *International Journal of Engineering and Technology*, *1*(1), 43–54.
- Kroll, L., Blau, P., Wabner, M., Frieß, U., Eulitz, J., & Klärner, M. (2011). Lightweight components for energy-efficient machine tools. *CIRP Journal of Manufacturing Science and Technology*, *4*(2), 148–160.
- Li, S. (2002). Gear contact model and loaded tooth contact analysis of a three-dimensional. *Thin-Rimmed Gear. Journal of Mechanical Design*, *124*(3), 511–517.
- Meneghetti, G., Dengo, C., & Lo Conte, F. (2018). Bending fatigue design of case-hardened gears based on test specimens. *Proceedings of the Institution of Mechanical Engineers, Part c: Journal of Mechanical Engineering Science*, *232*(11), 1953–1969.
- Oda, S., Nagamura, K., & Aoki, K. (1981). Stress analysis of thin rim spur gears by finite element method. *Bulletin of JSME*, *24*(193), 1273–1280.
- Petry-Johnson, T. T., Kahraman, A., Anderson, N. E., & Chase, D. R. (2008). An experimental investigation of spur gear efficiency. *Journal of Mechanical Design*, *130*(6), 062601.
- SIMULIA. (2013). “Abaqus 613,” *Analysis User's Guide*. Dassault Systems.
- Solomon, D. G., Greco, A., Masselli, C., Gundabattini, E., Rassiah, R. S., & Kuppan, R. (2020). A review on methods to reduce weight and to increase efficiency of electric motors using lightweight materials, novel manufacturing processes, magnetic materials and cooling methods. *Annales De Chimie: Science Des Matériaux*, *44*, 1–14.
- Xu, H., Kahraman, A., Anderson, N. E., & Maddock, D. G. (2007). Prediction of MECHANICAL EFFICIENCY OF PARALLEL-AXIS GEAR PAIRS. *ASME Journal of Mechanical Design*, *129*(12), 58–68.
- Drago, R. J., & Lutthans, R. V. (1983b). An experimental investigation of the combined effects of rim thickness and pitch diameter on spur gear tooth root and fillet stresses. (AGMA Paper P229.22, 1981)
- Drago, R. J., & Pizzigati, G.A. (1980). Some progress in the accurate evaluation of tooth root and fillet stresses in lightweight, Thin-Rimmed Gears. (AGMA Paper 229.21)
- Opalic, M., Vuckovic, K., & Kjjajin, M. (2011). Effect of web arrangement to thin-rim gear tooth contact stress. In: *15th International Research/Expert Conference*, Prague, Czech Republic.
- SAE International. (2017). SAE J 1619–2017, Single Tooth Gear Bending Fatigue Test. [Online]. Available at: https://www.sae.org/standards/content/j1619_201705/. Accessed 9 May 2023.
- SAE International. (n.d.). SAE J 821042, Gear Single Tooth Bending Fatigue Test. [Standard]. SAE Mobilus. https://doi.org/10.4271/j821_042
- Simon, V. (1981). Load capacity and efficiency of spur gears in regard to thermo-end lubrication. In: *International Symposium on Gearing and Power Transmissions*, Tokyo, Japan.

Publisher's Note Springer Nature remains neutral with regard to jurisdictional claims in published maps and institutional affiliations.